Effects of Alpha Particle Transport Driven by Alfvénic Instabilities on Proposed Burning Plasma Scenarios on ITER

G. Vlad 1), S. Briguglio 1), G. Fogaccia 1), F. Zonca 1), M. Schneider 2)

1) Ass. Euratom-ENEA sulla Fusione, C. R. Frascati, C.P. 65, 00044 Frascati, Rome, Italy
2) Ass. Euratom-CEA, CEA/Cadarache, 13108 Saint Paul-lez-Durance, France

e-mail contact of main author: vlad@frascati.enea.it

Abstract. The consistency of proposed burning plasma scenarios with Alfvénic instabilities driven by alpha particles is investigated. If the alpha particle pressure is above the threshold for resonant excitation of Energetic Particle driven Modes (EPMs), significant modification of the alpha particle pressure profile can take place. Model simulations are performed using the Hybrid MHD-Gyrokinetic Code (HMGC) retaining relevant thermal-plasma parameters, safety factor and alpha particle pressure profiles. ITER monotonic-q and reversed-shear scenarios are considered. A "hybrid" ITER scenario is also studied and quantitatively compared with the previous ones. We find that, unlike the latter, the former equilibria are unstable. Nonlinear effects on the alpha-particle pressure profile result, however, to be negligible for the monotonic-q case. They can instead be relevant for the reversed-shear scenario. The assessment of such a conclusion requires further investigations concerning the possibility that the strong EPM instability is regulated, in realistic conditions, by nonlinear effects of weaker Alfvén modes.

1. Introduction

In a burning plasma, energetic ions (as, e.g., alpha particles) are expected to transfer their energy via Coulomb collisions to the thermal plasma, thus providing a nuclear self-heating mechanism and a route to ignition. It is well known that, due to their super-Alfvénic speed, they can resonate with and possibly destabilize shear Alfvén modes. Energetic ion transport and confinement properties can in turn be affected by the nonlinear interaction with the Alfvénic modes themselves. Several evidences of rapid transient transport of energetic ions related with fluctuations in the Alfvén mode frequency range have been observed in plasmas heated by different auxiliary power systems as reported, e.g., in the JT-60U tokamak [1] in connection with the so called Abrupt Large amplitude Events (ALE). A comprehensive description of experimental observations of collective mode effects on fast ions is given in Ref. [2] and references therein. Meanwhile, particle-simulation studies have shown [3, 4, 5, 6] that energetic-ion redistribution can take place because of fast-growing Energetic Particle driven Modes (EPMs) [7].

On the other hand, the operation scenarios for next-step proposed burning-plasma experiments, such as ITER-FEAT [8, 9], are usually obtained from equilibrium and transport codes which do not include the physics required to describe shear Alfvén modes: the possibility that these are excited and, eventually, produce macroscopic transport of alpha particles themselves is neglected. Thus, consistency problems of the envisaged burning-plasma scenarios may occur, in particular with reference to the alpha-particle radial profile and, therefore, to the fusion power density. In this paper the stability of various ITER equilibria with respect to shear Alfvén waves is investigated by means of the Hybrid MHD-Gyrokinetic Code (HMGC)[3, 10, 11]. This simulation approach allows us to study the nonlinear evolution of unstable modes. Scenarios can be considered consistent with such nonlinear dynamics if alpha-particle pressure profiles in the presence of fully saturated modes are very close to the initial ones. On the contrary, strong differences between the profiles with and without shear-Alfvén mode dynamics could signify the inconsistency of the corresponding scenario, though a definitive assessment would require investigating how the results could be altered in the frame of a dynamic approach to the reference profiles. In fact, it cannot be ruled out by our simulations that the nonlinear saturation of weaker Alfvén modes, driven unstable when the alpha-particle pressure gradient has not yet reached the nominal scenario value, can regulate the stronger EPM dynamics, then reducing the overall alpha particle radial displacement. These cases would anyway require more detailed analysis in order to define the reference equilibrium profiles in a more realistic as well as reliable way.

2. The Model

The plasma model adopted in the HMGC code consists [3, 10, 11] of a thermal plasma and an energetic particle population. The former is described by reduced $O(\epsilon^3)$ MHD equations [12, 13] in the limit of zero pressure (ϵ being the inverse aspect ratio of the torus), including resistivity and viscosity terms; retaining only $O(\epsilon^3)$ terms allows one to investigate only equilibria with shifted circular magnetic surfaces. The energetic particle population is described by the nonlinear gyrokinetic Vlasov equation [14, 15], solved, by particle-in-cell (PIC) techniques, in the limit $k_\perp \rho_H \ll 1$ (with $k_\perp$ being the perpendicular-to-magnetic-field component of the wave vector, and ρ_H energetic-particle Larmor radius). Energetic particles and thermal plasma are coupled through the divergence of the energetic-particle pressure tensor, which enters the vorticity equation [16]. Numerical simulations are performed retaining, for each scenario, the relevant thermal-plasma quantities – the on-axis equilibrium magnetic field, major and minor radii, the safety-factor q, the plasma density n_e, the electron temperature T_e– and the alpha-particle density n_H. Energetic particles are loaded according to an isotropic slowing-down distribution function with an upper energy cut-off given by the fusion energy of alpha particles, and the critical energy E_c given by the Stix expression [17]. In the following we assume, for simplicity, $n_D = n_T = n_i/2$ and $n_i = n_e$; thus $E_c \simeq 33.0 T_e$. Here n_D, n_T, n_i are the deuterium, tritium and (total) bulk ion densities, respectively. We neglect, for simplicity, the nonlinear mode-mode coupling among different toroidal mode numbers, then limiting the analysis to the evolution of a single toroidal mode n, while keeping fully nonlinear dynamics for energetic particles. Fluid nonlinearities are not expected indeed to considerably alter EPM dynamics [3]. Note, however, that considering a single toroidal mode could underestimate the EPM effects on alpha-particle transport in the case of multi-n resonance overlap.

3. Results

Three different ITER-FEAT scenarios have been considered: the reference monotonic-q scenario (“scenario 2”, SC2), the reversed shear scenario (“scenario 4”, SC4) and a recently proposed “hybrid” scenario (“scenario H”, SCH). Data corresponding to the two former scenarios are available at the (ITER) Joint Work Site [18]; those related to SCH have been obtained by the package of simulation codes CRONOS [19].

SC2 is an inductive, 15 MA scenario, with 400 MW fusion power and fusion yield $Q = 10$. SC4 is a steady state, 9 MA, weak-negative shear scenario, with about 300 MW fusion power and $Q = 5$; the q profile is characterized by $q_{min} \simeq 2.4$ and $r_{q_{min}}/a \simeq 0.68$. SCH is a steady state, 11.3 MA weak-positive shear scenario, with about 400 MW fusion power and $Q \simeq 5$. Other significant plasma and device parameters are reported in Table I, while the radial profiles of the relevant quantities are shown in FIG. *1*. Note that, while β_{H0} changes within a factor 1.5 between the different scenarios (with SCH corresponding to the largest value, and SC4 to the smallest one), the maximum value of the local alpha particle drive $\alpha_{H,max} \equiv$

$\max\{-R_0 q^2 \beta_H'\}$ varies by more than a factor 7 (with SC4 and SC2 detaining the highest and lowest score, respectively). Here β_{H0} is the on-axis value of β_H, the ratio between alpha-particle and magnetic pressures, and "prime" denotes the radial derivative.

TABLE I: Plasma and device parameters for the three ITER-FEAT considered scenarios. Here a and R_0 are the minor and major radius of the torus, respectively, $q_{95\%}$ is the value of the safety factor at the surface where the poloidal flux is the 95% of the total, B_T is the on-axis toroidal magnetic field, n_{e0}, T_{e0}, n_{H0} and β_{H0} are the on-axis electron density, electron temperature, alpha-particle density and the ratio between alpha-particle and magnetic pressures, respectively, and $\alpha_{H,max}$ is the maximum value of the local alpha-particle drive, located at $r = r_{\alpha_{H,max}}$.

	SC2	SC4	SCH
a (m)	2.005	1.859	1.8017
R_0 (m)	6.195	6.34	6.3734
$q_{95\%}$	3.14	5.13	3.22
B_T (T)	5.3	5.183	5.3
n_{e0} ($10^{20}\mathrm{m}^{-3}$)	1.02	0.73	0.72
T_{e0} (keV)	24.8	23.9	30.0
n_{H0} ($10^{18}\mathrm{m}^{-3}$)	0.78	0.62	0.88
β_{H0} (%)	1.10	0.92	1.37
$\alpha_{H,max}$	0.085	0.600	0.155
$r_{\alpha_{H,max}}/a$	0.25	0.50	0.60

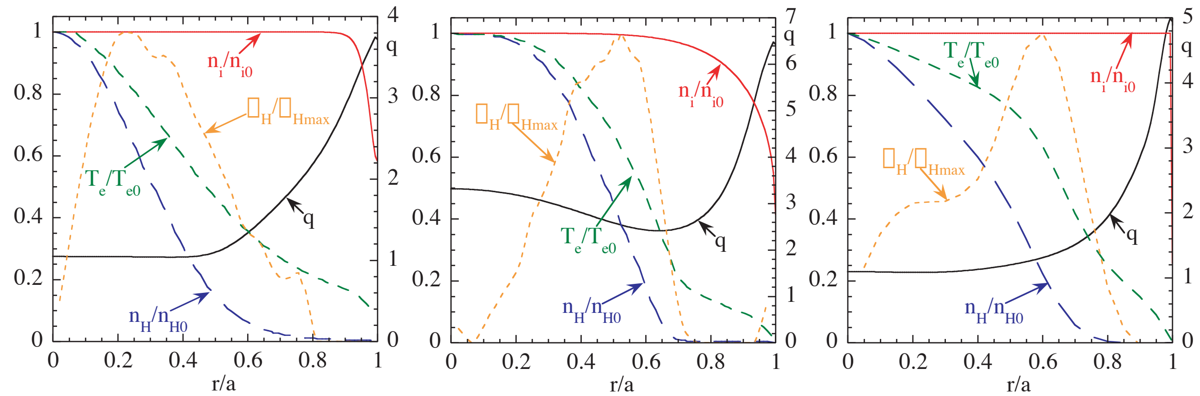

FIG. 1: Radial profiles of safety factor (q), normalized bulk-ion (n_i), and alpha-particle (n_H), densities, electron temperature (T_e), and alpha-particle local drive (α_H), for ITER-FEAT SC2 (left), SC4 (center) and SCH (right) scenarios.

3.1. Linear dynamics

Let us first consider the linear dynamics of the ITER-FEAT monotonic-q scenario (SC2), as it emerges from the first (low-field-amplitude) phase of the simulations. Several toroidal mode numbers, with $n \geq 2$, are found to be unstable. The most unstable one results to be $n = 4$, with a mode structure radially localized around $r/a \simeq 0.28$ (close to the position where the local drive α_H is maximum; see Table I). The mode has growth rate $\gamma/\omega_{A0} \simeq 0.023$ ($\omega_{A0} \equiv v_{A0}/R_0$ being the on-axis Alfvén frequency and v_{A0} the on-axis Alfvén velocity); its real frequency, $\omega/\omega_{A0} \simeq 0.067$, is below the lower Alfvén continuum (see FIG. 2 left). The latter feature allows us to identify the mode as a Global Alfvén Eigenmode (GAE) [20]. Note that the same scenario has been investigated in a previous paper [21], and found linearly stable; the different conclusions may be traced back to some differences between the equilibrium profiles considered here [18] and the ones used in ref. [21], obtained from ref. [22], and – also – to some approximations, adopted in ref. [21]: a Maxwellian distribution function instead of a slowing-down one (with parameters chosen to make the two as close as possible), and an inverse aspect ratio smaller than the actual one (with appropriate rescaling of the drive).

The analysis of the linear dynamics of the ITER-FEAT reversed shear scenario (SC4) shows that only the toroidal mode number $n = 2$ is unstable. The mode is radially localized around $r/a \simeq 0.44$ in a throat of the toroidal gap, with growth-rate $\gamma/\omega_{A0} \simeq 0.022$ and real frequency $\omega/\omega_{A0} \simeq 0.180$. Also in this case the radial localization of the mode is close to the radius where the local drive α_H is maximum (see Table I). A second mode, weaker than the first one ($\gamma/\omega_{A0} \simeq 0.017$ and $\omega/\omega_{A0} \simeq 0.070$), is also observable close to the q_{min} surface, just above the lower Alfvén continuum, resembling to the so-called Cascade mode [23] (see FIG. *2*, center).

Different from the previous cases, the ITER-FEAT hybrid scenario (SCH) corresponds to a stable configuration. In order to estimate its safety margins, we artificially increase β_{H0}, while keeping its profile and all the other quantities fixed, until EPMs are driven unstable. We analyze modes with $n \leq 8$. The lowest threshold for EPM instability occurs for $n = 8$, and it is given by $\beta_{H0,\mathrm{th}} \simeq 1.6\beta_{H0,\mathrm{SCH}}$. From these results we cannot rule out that modes with higher n are even more unstable. However, we find that the threshold dependence on n is already very weak for $n \approx 8$; therefore, we do not expect appreciable decrease of such threshold when further increasing n. Once again, the (virtually) unstable modes develop around a radial position ($r/a \simeq 0.57$) close to the maximum-α_H radius, with a real frequency $\omega/\omega_{A0} \simeq 0.25$, just below the toroidal gap (see FIG. *2* right, showing the results obtained for $\beta_{H0} \simeq 2.45\beta_{H0,\mathrm{SCH}}$).

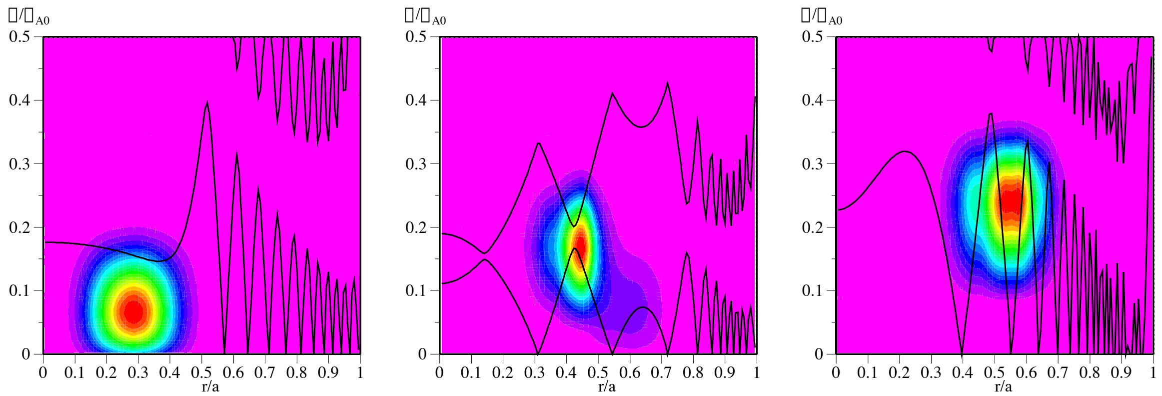

FIG. 2: Power spectra of scalar-potential fluctuations in the (r, ω) plane, during the linear phase, for the SC2 $n = 4$ (left), SC4 $n = 2$ (center) and SCH $n = 8$ (with $\beta_{H0} \simeq 2.45\beta_{H0,\mathrm{SCH}}$) (right) cases. Upper and lower Alfvén continuous spectra are also plotted (black).

We can adopt the same artifice of increasing the β_{H0} at values well above the reference value, in order to identify the dominant wave-particle resonances for these modes. Indeed, in the presence of a large drive, the mode will be less affected by damping mechanisms, and its frequency will be mainly determined by the relevant resonances. In FIG. *3*, we compare the frequency spectrum obtained for the SC4 $n = 2$ case (left) with that obtained for the same case, with an artificially high $\beta_{H0} \simeq 2.9\beta_{H0,\mathrm{SC4}}$ value (right). It seems that the mode is primarily driven by the precession resonance and the precession-bounce resonance of order $l = -1$, which are maximum at frequency $\omega = \bar{\omega}_d$ (green curve in FIG. *3*) and $\omega = \bar{\omega}_d - \omega_B$ (light blue curve), respectively, with

$$\bar{\omega}_d \simeq \frac{E_{\rm fus}}{m_H R_0 \omega_{cH}} \frac{nq(r)}{r} \, , \qquad \omega_B \simeq \frac{1}{R_0 q(r)} \sqrt{\frac{E_{\rm fus}}{m_H}} \left(\frac{r}{R_0} \right)^{1/2} \, ,$$

m_H and ω_{cH} the alpha-particle mass and cyclotron frequency, respectively, and $E_{\rm fus} = 3.52$ MeV. The transit resonance, maximum at frequency $\omega_t \simeq (E_{\rm fus}/2m_H)^{1/2}/q(r)R_0$ (yellow curve) does not seem to be effective. Noting that the precession frequency scales with n, this (preliminary) result would explain why, for all the examined scenarios, the most unstable modes are characterized by low or not too high values of n: we indeed expect that, when realistic values of β_{H0} are considered, the damping mechanisms become important, and the most unstable modes will be characterized by those (moderate) values of n that make the precession-bounce frequencies close to the damping-free gap region at the radius where α_H is maximum.

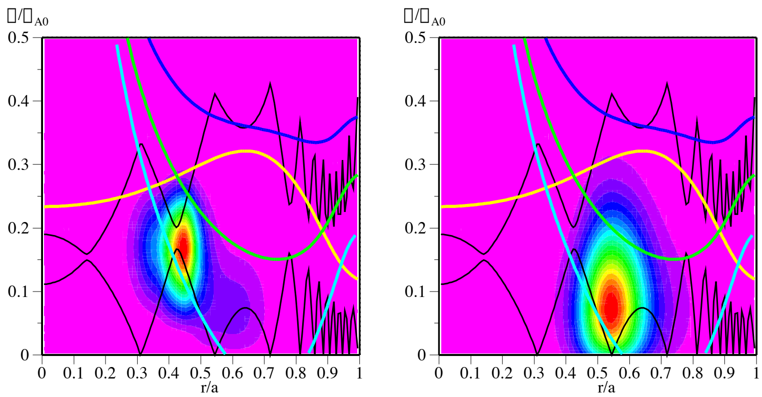

FIG. 3: Power spectra of scalar-potential fluctuations in the (r, ω) plane, during the linear phase, for SC4 scenario with $n = 2$. The reference case (left) is compared with the case obtained with an artificially high $\beta_{H0} \simeq 2.9\beta_{H0,{\rm SC4}}$ (right). The transit frequency (yellow) is also plotted, along with the precession frequency (green) and the precession-bounce frequencies of order +1 (dark blue) and -1 (light blue).

3.2. Nonlinear dynamics

It has been shown [4] that sufficiently unstable EPMs saturate through a rapid (few hundreds of Alfvén times) convection, generally yielding a sudden broadening of the energetic-particle pressure profile. This phase is followed by a slower one, during which the saturated electromagnetic fields act as a scattering mechanism for the energetic particles, producing their further diffusion [21]. However, the quantitative impact of these nonlinear phenomena on the alpha-particle confinement depends not only on the drive intensity, but also on its localization, the details of damping mechanisms and the alpha-particle transport, affected, in various ways, by other features of the equilibrium.

Figure *4* shows the effects of the nonlinear dynamics on the two unstable scenarios: SC2 (top) and SC4 (bottom). The frequency spectra resulting from the saturation of the EPMs are reported, for each scenario, along with the alpha-particle pressure profiles obtained at a certain time, during the diffusive phase. The initial pressure profiles are also reported, in order to appreciate the modifications introduced by the mode dynamics. We see that the monotonic-q (SC2) scenario is scarcely affected by the nonlinear saturation of the unstable modes (FIG. *4* top right). This feature can been understood by taking into account both the nature of GAE presented, in this case, by the most unstable mode (cf FIG. *2* left, which refers to the linear-dynamics phase) and the shape of the gap structure, which causes the mode to face a continuum-damping "barrier" in order to penetrate the outer region. In these conditions, the mode has no chance, in the nonlinear phase (FIG. *4* top left), to follow and further scatter the displaced particles. Moreover, the low value of the safety factor makes the characteristic width of the single-particle orbit quite small, making the residual diffusion very contained.

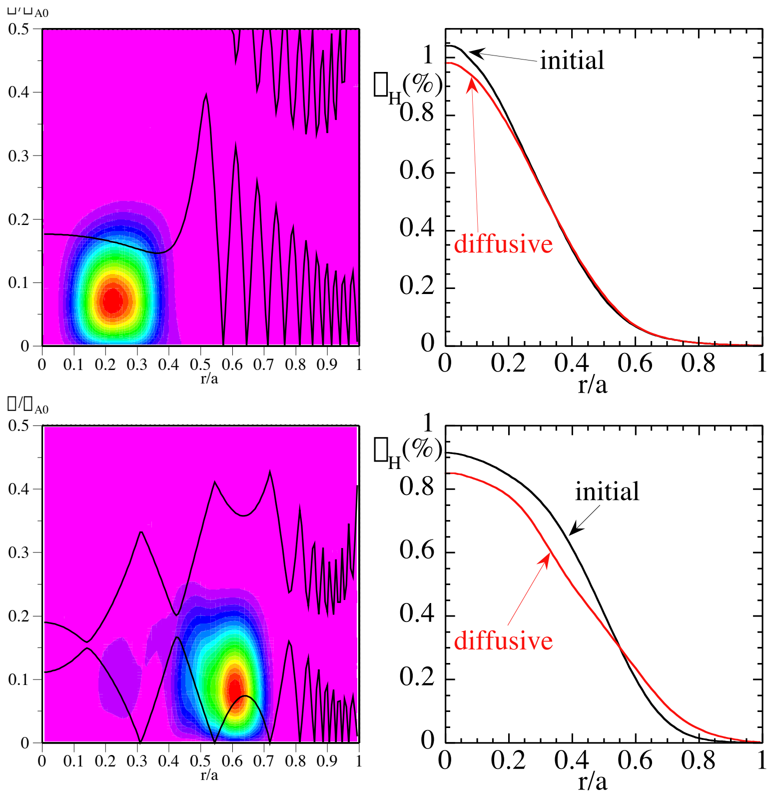

FIG. 4: Power spectra of scalar-potential fluctuations in the (r, ω) plane, during the diffusive phase ($\approx 200\,\omega_{A0}^{-1}$ after the nonlinear convection has completed), for the SC2 $n = 4$ (top left) and SC4 $n = 2$ (bottom left) cases. Corresponding alpha-particle pressure profiles are shown on the right (SC2, top, and SC4, bottom), and compared with the respective initial profiles.

The situation for the reversed-shear (SC4) scenario is quite different: both the initial localization of the mode inside the gap (cf FIG. *2* center) and the fair alignment of the gap itself allow the mode to saturate by reaching the outer q_{min} surface (FIG. *4* bottom left). Alpha particles, characterized by large orbit width, because of the large value of the safety factor q, can undergo a significant displacement in the convective phase and a strong scattering in the diffusion phase. The resulting saturated-phase β_H profile is quite broader than the initial one (FIG. *4*, bottom right).

We can give these results a quantitative form by introducing the (time dependent) quantity r_y, defined as the radial surface enclosing the fraction y of the alpha-particle energy content, and implicitly given by

$$\frac{\int_0^{r_y} r\beta_H(t,r)dr}{\int_0^a r\beta_{H,\mathrm{init}}(r)dr} = y\,.$$

Here, $\beta_H(t,r)$ is the energetic particle pressure profile at time t, while $\beta_{H,\mathrm{init}}(r)$ is the initial profile (i.e., before the nonlinear effects become important). We can then compare the values β_{H0} and $r_{95\%}$ in the initial stage with those obtained just after the nonlinear convection has completed. This is done, for SC2 and SC4, in Table II and Table III, respectively. The rates of variation of both quantities during the subsequent diffusive phase are also reported ($\tau^{-1}_{\mathrm{diff},\beta_{H0}}$ and $\tau^{-1}_{\mathrm{diff},95\%}$). Moreover, in order to give a measure of the sensitivity of these results to the drive intensity, additional (virtual) cases are considered, related to larger initial β_{H0} values.

TABLE II: Initial ("init") and just-after-convection values ("conv") of β_{H0} and $r_{95\%}$ for SC2 scenario, $n = 4$. Results for the reference case ($\beta_{H0} = \beta_{H0,\mathrm{SC2}}$) are shown in the first column, while those for artificially increased cases ($\beta_{H0} > \beta_{H0,\mathrm{SC2}}$) are shown in the second and third columns. The inverse of the characteristic diffusive times $\tau_{\mathrm{diff},\beta_{H0}}$ and $\tau_{\mathrm{diff},95\%}$ are also reported.

$\beta_{H0,\mathrm{init}}/\beta_{H0,\mathrm{SC2}}$	1.00	1.45	1.95
$\beta_{H0,\mathrm{conv}}/\beta_{H0,\mathrm{SC2}}$	0.94	1.20	1.34
$(\tau_{\mathrm{diff},\beta_{H0}}\omega_{A0})^{-1}$	4.6×10^{-5}	2.5×10^{-5}	5.8×10^{-4}
$r_{95\%,\mathrm{init}}/a$	0.62	0.62	0.62
$r_{95\%,\mathrm{conv}}/a$	0.63	0.63	0.64
$(\tau_{\mathrm{diff},95\%}\omega_{A0})^{-1}$	2.0×10^{-6}	6.1×10^{-7}	1.1×10^{-4}

TABLE III: Same as Table II for SC4 scenario, $n = 2$.

$\beta_{H0,\mathrm{init}}/\beta_{H0,\mathrm{SC4}}$	1.00	1.16	1.75
$\beta_{H0,\mathrm{conv}}/\beta_{H0,\mathrm{SC4}}$	0.97	1.07	1.40
$(\tau_{\mathrm{diff},\beta_{\mathrm{H0}}}\omega_{A0})^{-1}$	1.4×10^{-4}	4.3×10^{-4}	1.2×10^{-3}
$r_{95\%,\mathrm{init}}/a$	0.65	0.65	0.65
$r_{95\%,\mathrm{conv}}/a$	0.74	0.74	0.76
$(\tau_{\mathrm{diff},95\%}\omega_{A0})^{-1}$	5.2×10^{-4}	9.5×10^{-4}	2.4×10^{-3}

For both scenarios, we observe that increasing the initial alpha-particle pressure content above the reference value hardly affects the results relative to the global containment of alpha-particles, as far as the convective saturation is concerned: the ratio between $r_{95\%}$ before and after the convection varies very little when going from the reference to the virtual, large-β_{H0}, cases. On the opposite, a pronounced effect is obtained both on the nonlinear decrease of the on-axis β_H value and on the after-convection diffusion rates. This seems to be consistent with the fact that the overall convective effect is mainly determined by the capability of the mode structure of following the alpha-particles while displacing them outwardly; once the convection has started, this feature primarily depends on the gap structure and, eventually, on the position of the minimum-q surface. On the opposite, the fluctuating field level influences the alpha-particle transport, once the saturated mode structure is determined, both in flattening the pressure profile within the radial surface where the mode is localized after its saturation, and diffusing particles outside that surface.

4. Conclusions

In the present paper we have analyzed the consistency of proposed burning plasma ITER scenarios with the nonlinear dynamics of Alfvénic modes driven unstable by alpha particles, using a PIC simulation code (HMGC). Both the standard ITER-FEAT monotonic-q scenario and the reversed shear one result to be unstable at reference values of alpha-particle pressure. Nevertheless, nonlinear saturation of the most unstable mode produces negligible modification of the alpha particle radial profile for the monotonic-q scenario. Appreciable changes are instead observed for reversed-shear. The proposed hybrid scenario, on the contrary, is found stable at the reference value of alpha-particle pressure, with a safety margin of about 1.6 in the central pressure value.

Several points should be noted, before drawing definitive conclusions from these results. First, the fact that single toroidal mode number dynamics is considered can result in underestimating the effects of Alfvén modes. Indeed, energetic-particle displacement could be enhanced by the overlapping of different-n resonances. Second, and in the opposite sense, gyrokinetic PIC simulations truncated at $O(\omega^2/\omega_c^2)$ cannot reproduce in a realistic way the dynamics of a plasma discharge on the long transport scale [14]. The stability of a given scenario is then analyzed by *assuming* the reference equilibrium, i.e. without considering how its formation is affected by the Alfvén mode dynamics. A multi-scale dynamic approach could in principle reveal that, even in the most hazardous scenario (SC4), the fast EPM dynamics is moderated by the nonlinear effects produced by weaker Alfvén modes driven unstable while the alpha-particle pressure gradient is building up. If this were the case, the overall alpha-particle displacement could come out to be much weaker than that predicted by the present paper.

Such considerations do not alter, however, the conclusion that the reversed-shear SC4 scenario deserves to be further investigated in order to make it surely consistent with the Alfvén mode dynamics.

Acknowledgments: The authors wish to thanks Dr. L.G. Eriksson and Dr. F. Imbeaux for their support in preparing the ITER hybrid scenario.

[1] Shinohara, K., et al., Nucl. Fusion **41** (2001) 603; Shinohara, K., et al., Nucl. Fusion **42** (2002) 942.
[2] Heidbrink, W.W., Phys. Plasmas **9** (2002) 2113.
[3] Briguglio, S., et al., Phys. Plasmas **5** (1998) 3287.
[4] Briguglio, S., et al., Phys. Lett. A **302** (2002) 308.
[5] Vlad, G., et al., *29th EPS Conf.*, vol 26B (ECA) (2002) P-4.088.
[6] Zonca, F., et al., Phys. Plasmas **9** (2002) 4939.
[7] Chen, L., Phys. Plasmas **1** (1994) 1519.
[8] ITER Physics Basis Editors, et al., Nucl. Fusion **39** (1999) 2137.
[9] Aymar, R., et al., "ITER-FEAT-The future international burning plasma experiment overview", Fusion Energy 2000 (Proc. 18th Int. Conf. Sorrento, 2000), C&S Papers Series 8/C, IAEA (2001), CD-ROM file OV/1 and http://www.iaea.org/programmes/ripc/physics/fec2000/html/node1.htm.
[10] Vlad, G., et al., Phys. Plasmas **2** (1995) 418.
[11] Briguglio, S., et al., Phys. Plasmas **2** (1995) 3711.
[12] Strauss, H.R., Phys. Fluids **20** (1977) 1354.
[13] Izzo, R., et al., Phys. Fluids **26** (1983) 2240.
[14] Frieman, E.A., and Chen, L., Phys. Fluids **25** (1982) 502.
[15] Lee, W.W., J. Comp. Phys. **72** (1987) 243.
[16] Park, W., et al., Phys. Fluids B **4** (1992) 2033.
[17] Stix, T.H., Plasma Phys. **14** (1972) 367.
[18] ftp://itergps.naka.jaeri.go.jp/PF_control/EQDSK_files/...
[19] Basiuk, V., et al., Nucl. Fusion **43** (2003) 822-830.
[20] Appert, K., et al., Plasma Phys. **24** (1982) 1147.
[21] Vlad, G., et al., Plasma Phys. Contr. Fusion, **46** (2004) S81-S93.
[22] Budny, R.V., Nucl. Fusion **42** (2002) 1383.
[23] Sharapov, S.E., et al., Phys. Lett. **A289** (2001) 127.